A Velocity Based Boundary Element Method with Modified Trailing Edge for Prediction of the Partial Cavities on the Wings and Propeller Blades

Alexander S. Achkinadze,
Department of Theory of Ship, State Marine Technical University, St Petersburg, Russia,
Vladimir I. Krasilnikov,
Department of Ship Performance, MARINTEK Sintef Group, Trondheim, Norway

Abstract
This paper presents a new velocity based boundary element method for calculation of the partial cavities on the wings and propeller blades. The fully correct mathematical formulation of the problem about cavitating bodies is characteristic feature of the developed method and numerical algorithm. The special algorithm of Modified Trailing Edge (MTE) is used for definition of the lifting (circulation) part of the flow. MTE tool allows the approximate accounting for viscous effects on lift and pressure distribution. The miscellaneous cavity closure model is recommended for calculation. The prediction of the cavity patterns is performed using Iterative Cavity Alignment (ICA) procedure with Free Cavity Length (FCL). The results of the test calculations and comparisons with experimental data are given in the paper.

1. Introduction

The great amount of the investigations has been done during last years on numerical simulation of the cavitating flow around wings and propellers. The questionnaire undertaken by ITTC Committee (1999) shows the diversity of the analysis procedures from lifting-surface theory (Lee C.-S (1979), Achkinadze & Narvsky (1987), Ishii (1992), Szantyr (1994)) through boundary element methods (Lee J.-T. (1987), Uhlman (1987), Kinnas & Fine (1993), Kim (1995), Mueller & Kinnas (1997)) and up to RANS solutions (Rebound & Delannoy (1994), Hsiao & Pauley (1998)). Obviously, today BEM methods seem to be the most efficient in practical calculations, because they naturally solve the problem of the leading edge and thickness effects and, at the same time, are not so exacting to computational resources and model tuning as RANS solvers.

In spite of the so-called potential based methods are the most common in partially cavitating body problem (Lee J.-T. (1987), Kinnas & Fine (1993), Mueller & Kinnas (1997)), these methods have the definite drawbacks. The necessity of the iterative satisfaction of the non-linear Kutta-Jowkovski condition at the trailing edge and unavoidable procedure of the numerical differentiation when defining the velocities from potential values decrease the computational efficiency of the potential based algorithms. The additional difficulties occur in the cavitation problem when the dynamic boundary condition on the cavity surface results in Fredgolm integral equation of the 1st kind within potential based method (Dang & Kuiper (1998)). From this point of view the velocity based "vortex" BEM (Alexandrov (1978), Uhlman (1987), Rowe & Blottiaux (1993)) are more preferable. It use the only vortices distributed on the boundary surface and provide the Fredgolm equation of the 2nd kind on the cavity surface implying the absence of the relative motion of fluid inside the boundary surface. However, this assumption is not valid for rotating bodies like propeller blades (Mishkevich (1997)). Therefore the "vortex" method could not be applied to cavitating propeller problem at all. In this paper the authors make an effort to solve the mentioned problems using original velocity based BEM with Modified Trailing Edge. It could be considered as advance of the panel methods by Maslov (1974), Hess & Valarezo (1985), Ando et. al. (1998) and Narayana (1998). According to this approach the sources are distributed on the boundary surface while vortices are placed on the mean surface and wake behind the body (in the 3D case).

The fully correct formulation and form of the main integral equations as Fredgolm-type of the 2nd kind for kinematic boundary condition on the wetted surface and singular of the 1st kind for dynamic condition on the cavity surface make this method the most rigorous mathematically among other BEM. The algorithm of the Modified Trailing Edge (MTE) allows the convenient separation of the thickness and lifting (circulation) parts of the problem and direct satisfaction the Kutta-Jowkovski condition unlike iterative way.

Presumably, there is no universal cavity closure model suitable for all cases (Rowe & Blottiaux (1993), Kinnas (1998), ITTC Committee (1999)). Studying the different examples on 2D foils and keeping in mind the known paradox by Geurst (1956) the authors have concluded about miscellaneous closure model to be recommended for practical calculations. It implies the change between closed and open models in dependence upon the calculated cavity length. The

both models use the same system of the boundary conditions with coupled kinematic/dynamic condition on the cavity nose panel and without any conditions on the cavity end panel, that connects with the chosen class of the searched source strength function.
Although the full modeling of the cavitating wing or propeller requires the 3D formulation the simplified method of the equivalent 2D cavitating profile could be applied for prediction of the cavity extent on the body sections in practical calculations. The results of the comparative calculations presented in the paper illustrate the capabilities of the new method and give the estimation of the closed and open cavity models from the point of view of concordance with experimental data.

2. Formulation of the problem about partially cavitating body

Let us consider the ideal incompressible steady flow around body. The velocity field in the environment is described by the following vectors: V_R - total relative velocity of fluid, V_E - transferal velocity of the given point on the body surface, W - velocity induced by the body and cavities, V_ψ - inflow velocity, which is assumed to be pre-set in the present theory. The velocity vectors listed above are related by the following identity (Kochin et.al (1963)):

$$W + V_\psi = V_R + V_E \,. \tag{1}$$

The general system of the equations that describe the considered flow consists of Euler equation, which, in the given case, has the solution known as Bernoulli identity

$$p^* - p_A = -\frac{\rho\left(V_R^2 - V_E^2\right)}{2} + \rho g h \,, \tag{2}$$

where p* – absolute total pressure (with accounting for gravity forces), p_A - atmospheric pressure, h - immersion of the considered point under free surface, and continuity equation, which could be reduced to Laplace equation due to assumption about potential character of the inflow and induced velocity fields

$$\Delta\varphi = 0 \,, \tag{3}$$

where φ – perturbation velocity potential.
The following kinematic and dynamic boundary conditions are imposed.
Kinematic boundary condition ("no flow") on the wetted body surface S_{WET}:

$$\vec{V}_R \cdot \vec{n} = 0 \quad on\ S_{WET} \,. \tag{4}$$

Condition of the vanishing of the absolute velocities in the infinity outside the vortex wake (for 3D case):

$$W, V_\psi \to \frac{1}{\Re^{2+\kappa}} \quad at\ \Re \to \infty, \kappa > 0 \,, \tag{5}$$

where $\Re$ – distance from origin of the body-fixed coordinate system to considered point. In the 2D problem the degree exponent is less on 1.
Additional kinematic condition on the Modified Trailing Edge (MTE), which is the short tail added after realistic trailing edge of the body:

$$V_R \cdot n_{MTE} = 0 \quad on\ S_{MTE} \tag{6}$$

Formally this condition is "no flow" across the MTE surface, while in fact it fulfills the Kutta-Jowkovski condition about equality of the pressure values upper and below trailing edge point. The latter condition requires more detail explanations. As a matter of fact, any simulation of the trailing edge as sharp (or as the point of zero thickness) is the sort of schematization. In the reality we should consider the 3D flow around thick trailing edge where vortex sheets S^U_{FVS} and S^L_{FVS} start at the points M^U and M^L as shown on Figure 1a.

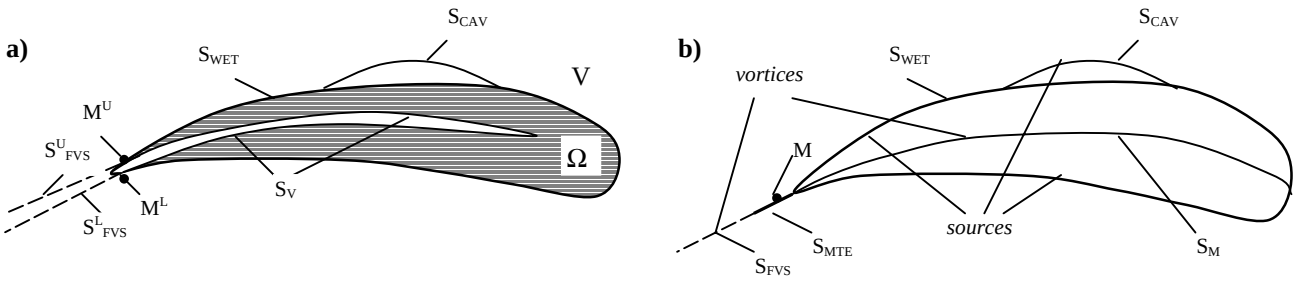

Figure 1. On formulation of the problem and derivation of the main integral equations.

Points M^U and M^L correspond to upper and lower sides of the thick trailing edge (rigorously, they should be taken with accounting for displacement thickness of the boundary layer on the body surface). The surfaces S^U_{FVS} and S^L_{FVS} are assumed to be rather long, but restricted by start vortices in the wake behind body. Within the potential frameworks they also have to be considered as thin, two-side surfaces, which join with conditioned vortex surface S_V inside body at the M^U and M^L points. The whole considered flow becomes to be divided on two domains by the boundary $S=S_{WET}+S^U_{FVS}+S^L_{FVS}+S_V$: external domain V with realistic flow and internal domain Ω with fictive flow. Thus, condition (6) defines the direction of the total velocity at the M^U and M^L points. As it will be shown in the section 3 the developed method allows the flow model, in which M^U coincides with M^L, while MTE itself appears to be so-called reciprocal (or return) point. In its turn, it allows us to avoid the known difficulties and satisfy the Kutta-Jowkovski condition directly, but not in the iterative way, unlike the panel methods based on perturbation potential formulation.

If consider the cavitation flow the *dynamic boundary condition on the cavity surface* S_{CAV} is required whilst kinematic "no flow" condition on this part of the body has to be taken off. Without any simplifications the dynamic condition on S_{CAV} is thought as equality of the absolute total pressure p* and vapour pressure p_V, i.e.

$$p^* = p_V \quad on\ S_{CAV}\,. \tag{7}$$

If substitute p* according to Bernoulli identity (2) in equation (7) after easy transformations one can obtain

$$V_R^2 = V_E^2\left(1+\sigma_Z\right), \tag{8}$$

where $\sigma_Z = 2\left(p_A + \rho g h - p_V\right)/(\rho V_E^2)$ is local cavitation number.

The main difficulty of the cavitation problem consists in the unknown beforehand domain where dynamic condition (8) has to be imposed. The direction and modulus of the total relative velocity V_R are also unknown. In the present BEM the first problem is solved by the iterative way. In order to get the definite projection of the total velocity the linearization of the dynamic condition is necessary. In the BEM it is reasonable to linearize the considered condition along the direction of the tangent to body surface at the given spanwise section. If designate this direction by index τ and corresponded unit vector as i_τ one can write the following asymptotic identity, which is valid for small quantities of the second order

$$(V_R \cdot i_\tau)^2 = V_E^2\left(1+\sigma_Z\right) \quad on\ S_{CAV} \tag{9}$$

Square root operation applied to both sides of (9) yields with accounting for (1)

$$W \cdot i_\tau = V_E \cdot i_\tau - V_\psi \cdot i_\tau + V_E\sqrt{1+\sigma_Z}\,. \tag{10}$$

3. Main integral equations

3.1. Fully wetted conditions

Application of the divergence theorem to flow domain (which consists of two sub-domains V (external) and Ω (internal) and boundary surface S_V) results in main integral Green's identity

$$kU(P_1) = -\int_S \frac{\partial U}{\partial n}\left(\frac{1}{R}\right)ds + \int_S U\frac{\partial}{\partial n}\left(\frac{1}{R}\right)ds\,, \tag{11}$$

where R – distance, U – harmonic function and coefficient k is: $k=4\pi$, if control point P_1 locates in the external domain V; $k=2\pi$, if P_1 locates on the boundary surface S; k=0, if P_1 appears in the internal domain Ω.

If require $U=\varphi$, $k=2\pi$, $\dfrac{\partial U}{\partial n} = \left(V_E - V_\psi\right)\cdot n$ for all points on S_{WET} one can obtain the Fredgolm's integral equation of the 2nd kind, which expresses the kinematic boundary condition and is common for most of the potential based BEM. Such equation is quite convenient for numerical solution, although the potential based BEM have their drawbacks. They are following. It is necessary to perform the numerical differentiation when define the velocity through potential φ values obtained from integral equation. Quite coarse approximation of the distributed doublet strength as constant within each element makes these methods close to discrete vortex/lattice approach. Many authors point out the definite difficulties connected with satisfaction of the Kutta-Jowkovski condition. Commonly, the additional iterative process is incorporated in the algorithm to achieve the desirable upper/lower pressure equality. In this sense the velocity based BEM seem to be more preferable. The easiest way to obtain the integral equation of the velocity based BEM is direct differentiation of (11) along surface normal direction at $k=4\pi$. However, the corresponded equation appears to be singular that is not convenient for numerical solution and evenly criticized by the adherents of the potential based BEM (Lee (1987)). The authors' approach allows the derivation of the integral equation in such a way it would be of the 2nd kind.

Let us write the integral Green's identity for internal domain Ω where k=0 and flow is characterized by U′ function:

$$0 = -\int_S \frac{\partial U'}{\partial n}\left(\frac{1}{R}\right)ds + \int_S U'\frac{\partial}{\partial n}\left(\frac{1}{R}\right)ds\,. \tag{12}$$

The normal directs inward body in (12) to be external regarding domain **Ω**. If change the direction of the normal and summarize (11) and (12) one can obtain

$$kU(P_1) = -\int_S \left(\frac{\partial U}{\partial n} - \frac{\partial U'}{\partial n}\right)\left(\frac{1}{R}\right)ds + \int_S (U - U')\frac{\partial}{\partial n}\left(\frac{1}{R}\right)ds\,. \tag{13}$$

Then we perform the differentiation of (13) in direction of the surface normal and come to

$$4\pi\frac{\partial U(P_1)}{\partial n} = 2\pi\left(\frac{\partial U}{\partial n} - \frac{\partial U'}{\partial n}\right) - \int_S \left(\frac{\partial U}{\partial n} - \frac{\partial U'}{\partial n}\right)\frac{\partial}{\partial n}\left(\frac{1}{R}\right)ds + \int_S (U - U')\frac{\partial^2}{\partial n\partial n}\left(\frac{1}{R}\right)ds\,. \tag{14}$$

The following conditions are imposed on identity (14).

$$\left.\begin{aligned} &U = \varphi \quad in\ V \\ &\frac{\partial\varphi}{\partial n} = (V_E - V_\psi)\cdot n \quad on\ S_Q = S_{WET} + S_{CAV} \\ &U = U' \quad on\ S_Q = S_{WET} + S_{CAV} \end{aligned}\right\}. \tag{15}$$

The source/sink layer of strength $q = \frac{\partial U}{\partial n} - \frac{\partial U'}{\partial n}$ is placed on S_Q surface to simulate the thickness effects.

$$\frac{\partial U}{\partial n} = \frac{\partial U'}{\partial n}\ on\ S_\sigma = S_V + S_{FVS}^{U+} + S_{FVS}^{U-} + S_{FVS}^{L+} + S_{FVS}^{L-}\,. \tag{16}$$

The doublet (vortex) layer of strength $\sigma = U - U'$ is placed on surface S_σ to simulate the lift effects. In result we come to main integral equation of the no-cavitation problem:

$$\frac{q}{2} - \frac{1}{4\pi}\int_{S_Q} q\frac{\partial}{\partial n}\left(\frac{1}{R}\right)ds + \frac{1}{4\pi}\int_{S_\sigma}\sigma\frac{\partial^2}{\partial n\partial n}\left(\frac{1}{R}\right)ds = (V_E - V_\psi)\cdot n \quad on\ S_Q\,. \tag{17}$$

The following principal features of the obtained equation have to be noted. The source/sink layer are placed on the wetted surface of the body while doublets (vortices) are distributed on the surface S_σ, which includes surface S_V inside body and trailing vortex sheets S^U_{FVS} and S^L_{FVS}. If doublet strength on S_σ is known, then (17) is Fredgolms' integral equation of the 2nd kind regarding q. In the present method it is achieved due to transformation of the vortex wake surfaces in one thin free vortex surface (FVS), which starts just after modified trailing edge point M where points M^U and M^L are superposed. Respectively, surface S_V inside body is reshaped in the mean surface as it is shown on Figure 1b. Such transformation is absolutely correct because no superposition of the considered domains appear while strength of the distributed singularities is simply defined as summa. The chordwise distribution of the doublets could be assigned arbitrary in the present method. When we consider the external flow domain it is not important how the doublets are distributed inside body because the only total circulation value defines the lift effects. This circulation has to be calculated as integral along the closed-up contour that intersects the surface S_σ in one point M on the MTE.

In the present work the easiest linear chordwise distribution of the doublets has been adopted

$$\sigma(\xi) = \frac{(\xi - \xi_{LE})}{(\xi_{TE} - \xi_{LE})}\Gamma \quad at\ \xi_{TE} \le \xi \le \xi_{LE}\,. \tag{18}$$

where ξ - chordwise coordinate, Γ - circulation around given section on the body span. The unknown values of Γ are defined from additional kinematic condition applied to MTE surface (6).

The following numerical algorithm appears more compact, if rewrite the main integral equation in terms of vortices instead of doublets using well-known identity between their strengths (Kochin et.al. (1963))

$$\gamma = n_\sigma \times grad\sigma\,, \tag{19}$$

where n_σ - normal to S_σ surface, and Biot-Savard formula. It yields

$$\frac{q}{2} + \frac{1}{4\pi}\int_{S_Q} q\frac{n\cdot R}{R^3}ds + \frac{1}{4\pi}\int_{S_\sigma}\frac{\gamma\cdot[R\times n]}{R^3}ds + \frac{1}{4\pi}\int_{L_\sigma}\frac{\Gamma_L dl\cdot[R\times n]}{R^3} = (V_E - V_\psi)\cdot n \quad on\ S_Q + S_{MTE}\,. \tag{20}$$

The third item in the left-hand part of (23) outcomes from Biot-Savard formula in the case when σ (or γ) function has "jumps" or non-zero values on the bounds of S_σ surface. It takes place, for instance, at the root section of the propeller blade if hub circulation is non-zero. This equation should be applied to wetted body surface and MTE.

3.2. Cavitating flow

At cavitation the equation (20) conforms on the wetted surface while the dynamic condition (10) has to be satisfied in the cavity domains S_{CAV}. By analogy with (20) the dynamic condition is written as follows

$$\frac{1}{4\pi}\int_{S_Q} q\frac{i_\tau \cdot R}{R^3}ds+\frac{1}{4\pi}\int_{S_\sigma}\frac{\gamma\cdot\left[R\times i_\tau\right]}{R^3}ds+\frac{1}{4\pi}\int_{L_\sigma}\frac{\Gamma_L dl\cdot\left[R\times i_\tau\right]}{R^3}=V_E\cdot i_\tau - V_\psi\cdot i_\tau + V_E\sqrt{1+\sigma_Z}\quad on\ S_{CAV}\,. \tag{21}$$

Likewise, in the cavitation problem we have obtained the system of two integral equations (20)-(21). The main characteristic feature of this system, in particular, and of the authors' method, in general, consists in absolutely correct formulation of the problem. Equation (20) is the Fredgolm-type integral equation of the 2nd kind regarding unknown source/sink strength q. It answers the correct formulation due to Fredgolm's alternatives. Equation (21) is singular integral equation of the 1st kind regarding q. In spite of it this equation answers the correct formulation because it is not restricted by Fredgolm's alternatives due to its singularity. It is only necessary to assume the smoothness of the searched function and specify the behaviour of the function at the bounds of integration domain. In other words, it is necessary to specify the class of the function for solution. In the considered case the choice of the proper class is caused by adopted cavity closure and detachment conditions.

4. Numerical solution

4.1. Discretization of the body surface

In order to reduce the integral equations (20)-(21) to the system of the linear algebraic equations (SLAE) the following representation of the body surface is used. The chord surface of the body (wing or propeller blade) is divided on the rectangular elements, which form the grid K×M (K – number of the elements on the span, M – number of the elements on the chord). The grid nodes define the vertices of the curvilinear boundary elements on the body surface. The using of the curvilinear elements is the important feature of the present method that allows us to achieve the better approximation of the most "hard" domains like leading edge and blade tip without significant increase of the number of the elements (Achkinadze & Krasilnikov (2001), Achkinadze et.al. (2001)). The using of the non-uniform cosine-space grid also helps in this deal. The following formulas define the location of the cosine-space grid nodes

$$\left.\begin{aligned} r_G(i) &= \left[1-\cos(\pi(i-1)/K)\right](l/2),\ i=1,\ldots,K \\ x_G(j) &= \left[1-\cos(\pi(j-1)/M)\right](c/2),\ j=1,\ldots,M \end{aligned}\right\}, \tag{22}$$

where l – span size, c – chord length.

The quite accurate and universal approximation of the body surface could be achieved using surface B-splines. The B-splines of the 4th order with special conditions accounting for behaviour of the functions at the interval bounds have been used in the both authors' propeller and wing codes. The mathematical tool of the curvilinear boundary elements is described in Achkinadze et.al. (2001). Here we only note that in the 2D case the using of the flat panels is more efficient. It allows the application of the analytical identities for straightforward source and vortex segments and significantly saves the computation time. But even in this case the accurate spline-approximation of the 2D foil surface near the edges is very desirable when one defines the flat panel nodes. The following parameters accounting for behaviour of the thickness chordwise distribution could be recommended for construction of the B-spline interpolant:

Round leading edge and sharp trailing edge

$$t = 2\arccos(-0.5-\xi/c)-\pi\,, \tag{23}$$

Both leading and trailing edge are round

$$t = 2\arccos(-2\xi/c)\,, \tag{24}$$

where $\xi/c\in$ [-0.5;0.5], $t\in$ [0;π].

The grid strips between two adjacent spanwise coordinates (r_G=const) form the additional auxiliary grid on the mean surface, where vortices are placed. The same strips define the spanwise size of the MTE panels, on which "no flow" condition is satisfied. The unknown source strength is assumed to be constant within each boundary element. Thus, total number of the unknown q is equal to number of the boundary elements. The piecewise linear representation of the spanwise circulation distribution is adopted. It specifies the additional unknown node-values of the circulation Γ. In order to provide the desirable smooth distribution of the Γ at relatively small number of the boundary elements the additional least-square-type smoothing procedure has been included in the SLAE solver in the propeller analysis algorithm. It uses the special polynomial representation of the Γ and is described in Achkinadze et.al. (2001).

4.2. Modified trailing edge

The MTE panels are defined as continuation of the mean surface from condition of the equal tangents to MTE and mean surface at the realistic trailing edge point, i.e.

$$\beta_{MTE}(r) = arctg\left(\partial Y_\sigma / \partial \xi\right) \quad at\ \xi = \xi_{TE}\ . \tag{25}$$

In the 2D case it is simply straightforward segment while in the 3D problem it is curvilinear surface that answers the condition (25) at the each spanwise section. The length of the MTE panel amounts 2% of the section chord length. Such definition corresponds to pure potential solution. It has to be noted that MTE tool could be useful as the easiest method accounting for viscous effects. Due to proper choice of the MTE bevel angle one can achieve the reduction of the calculated circulation that captures the influence of the viscosity. It seems to be obvious that proper β_{MTE} value has to provide the same lift coefficient C_L in the ideal solution as one in the viscous flow C_{LV}. C_{LV} could be obtained from 2D viscous calculation of the section profile or taken approximately using empiric identities. As it has been found during 2D test calculations the approximate formula proposed by Mishkevich (1994) for NACA,a=0.8/66mod sections allows the reasonable estimation of the C_{LV} in quite wide range of the section parameters and even could be used for other types of the sections. At fixed length of the MTE L_{MTE}=0.02c the problem about search of the bevel angle is reduced to solution of the non-linear equation

$$C_L\left(\beta_{MTE}, L_{MTE}\right) = C_{LV}\ , \tag{26}$$

which is treated by common half-division technique on prescribed range of the β_{MTE} values [-15°;+15°]. The using of the MTE tool for viscous corrections is illustrated in the section 5.1 for NACA4412 foils.

In the 3D case the problem of the accounting for viscosity is much more difficult. However, the same 2D algorithm described above could be applied here as well. The difference consists in using of the some equivalent 2D profile instead of realistic wing or blade section. There are different conditions of such equivalence (Zavadovski & Rusetsky (1988)). In authors opinion the following conditions could be recommended in the considered case:

1) equivalent profile has the same chordwise thickness distribution as one of realistic section;
2) normalized camber distribution (but not absolute maximum camber) coincides with one of realistic section;
3) maximum camber and angle of attack for equivalent profile are defined from following equations

$$\left.\begin{aligned} C_L\left(\alpha_{EQ}, \delta_{CEQ}\right) &= C_L^{3D} \\ C_m\left(\alpha_{EQ}, \delta_{CEQ}\right) &= C_m^{3D} \end{aligned}\right\}, \tag{27}$$

which provide the equality of the lift and moment of the equivalent profile and realistic section from 3D calculation. System (27) is solved by the iterative way. On the each iteration BEM solution of the profile is carried out at given α_{EQ}, δ_{CEQ} values. In the global algorithm this procedure precedes the β_{MTE} viscous correction by (26).

4.3. Cavity closure and detachment conditions

If the cavity bound is defined from equation of the streamline after solution of the system (20)-(21) then cavity trailing and leading ends should be under additional conditions. These conditions define the cavity model adopted for numerical algorithm. There are different cavity closure models suitable for BEM. The Riabouchinsky-type model with cavity termination as vertical plate has been used in the classical paper by Uhlman (1987). The modified Riabouchinsky model with fictive close-up curvilinear body has been proposed by Ivanov (1980) and applied by Alexandrov (1978) for partially cavitating foils using surface singularity method. Lemmonier & Rowe (1988) and Kinnas & Fine (1993) have adopted the so-called closed model with near wake, where the contradiction of having stagnation pressure at the cavity end is removed due to adding of the empiric wake zone behind cavity tail. In general these simplest model types work well for relatively short cavities (not more than 50% of chord length) and give the unrealistic results for long cavities (ITTC Committee (1999)). The principal drawback of the closed models consists in the so-called paradox by Geurst (1956), which appears when cavity end approaches to trailing edge (Achkinadze (2001)). The open cavity model is equally good for long partial cavities and super cavities. It has been applied by Achkinadze & Narvsky (1980, 1987), Achkinadze & Fridman (1994, 1998) and Yamaguchi & Kato (1983) (with improved collapsing region). The application of the Efros-type model with re-entrant jet in the BEM algorithm is known from paper by Dang & Kuiper (1998). Rowe & Blottiaux (1993) have applied different types of the closed and open models in their theory/experiment comparisons and have concluded that there is no universal model capable to provide the acceptable results in all possible cases. The authors can agree with this conclusion and recommend the so-called miscellaneous computation scheme in the practical calculations. It implies the change of the closure condition in dependence upon location of the cavity end. The location of the cavity termination point x_{CT}, which answers the change of the cavity model, is external prescribed parameter. If cavity is shorter than this prescribed value then closed model is used. If closed and open model both show the cavity longer than x_{CT} then open model result is accepted. In the intermediate case, when open model prediction is less than x_{CT} while closed model gives cavity length greater than x_{CT}, no any closure conditions are fulfilled. The dynamic boundary

condition is required up to x_{CT} location. The termination point is "free" parameter, which could be adjusted in order to achieve the better agreement with experiment as to certain integral characteristic.
The closed cavity model used in the authors' algorithm is similar to modified Riabouchinsky-type model with fictive close-up body. But unlike method by Ivanov-Alexandrov the simple straight segment is used instead of curvilinear body. The length and inclination of this segment regarding body surface is defined in iterations during Iterative Cavity Alignment (ICA) procedure as described in section 4.5. The condition for search of the cavity end point consist in the equality of the ordinates of the cavity bound (calculated streamline) and body surface at the closure point. The open model differs from described above by absence of any close-up bodies and requires the equality of the curvature of the cavity and body surfaces (or parallelism of the upper and lower cavity surfaces in the case of supercavitation) at the cavity end point (mathematically, equality of the tangent angles to both surfaces). In fact, at this point cavity bound smoothly goes downstream in the wake.

In the most of the numerical methods the cavity detachment point is simply prescribed at the leading edge or at the minimum pressure location (ITTC Committee (1999)). The authors use the similar assumption at first iteration and accept the cavity detachment in the point where $-Cp=\sigma$ in the fully wetted conditions. Then the location of the cavity detachment is elaborated during ICA iterations from Brillouin-Villat condition about equal curvature of the cavity bound and body surface at the detachment point.

4.4. System of the boundary conditions

The satisfaction of the boundary conditions in the cavity domain connects with the choice of the cavity model and class of the source strength function q. In order to provide the mathematically correct solution and meet the required class of q the following system of the boundary conditions is imposed (see also Figure 2). On the wetted body domain the kinematic condition (20) is satisfied. On the cavity nose panel the both kinematic (20) and dynamic (21) conditions are required. The dynamic condition (21) is satisfied everywhere inside cavity domain excluding end (closure) panel. There are no any conditions on the cavity end panel. The additional "no flow" condition is applied to MTE panel as described above to define the unknown circulation values.

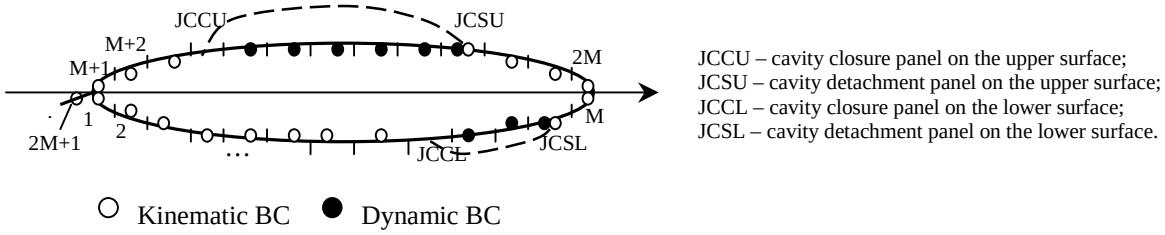

Figure 2. System of the boundary conditions (linearized step).

4.5. Iterative cavity alignment procedure with free cavity length

The cavitation number σ_Z is prescribed quantity in the present method while cavity length is unknown. Such methods are referred in ITTC Committee (1999) as methods with Free Cavity Length (FCL). The Iterative Cavity Alignment (ICA) procedure with FCL is used for evaluation of the ordinates of the cavity on two last steps of the calculation algorithm. Its general structure is following.

1) Calculation of the body at fully wetted conditions.
2) Checking of the $-Cp=\sigma$ condition and definition of the assumed cavity domains. Cavity nose and end points are taken in the points where $-Cp=\sigma$ in the fully wetted solution.
3) First-stage (linearized) calculation of the cavities with use of ICA procedure with FCL; singularities are placed on the body surface, boundary conditions are satisfied on the body surface.
4) Second-stage (non-linear) calculation of the cavities with use of ICA procedure with FCL; singularities are placed on the cavity surface (and fictive close-up segment in the closed model), boundary conditions are satisfied on the cavity surface, wetted body surface (and fictive close-up segment in the closed model).

The both 3rd and 4th steps use the same ICA procedure, which allows the automatic rebuilding of the cavity during iterations as to search of the cavity end and nose panels. The difference between closed and open models is reduced to different closure conditions to be checked at the end current panel as described in 4.3. The remaining part of the procedure is absolutely identical. There are no any conditions checked in the intermediate case between closed and open models. Here the location of the JCCU panel is defined by the location of the cavity termination point x_{CT}.

At present the described algorithm realized for 2D foil problem assumes the simultaneous consideration of the cavities on the upper and lower surfaces. It is important that both upper and lower cavities are considered simultaneously in the solution, because of better simulation of the flow picture around cavitating body. The separate consideration of the cavities with further iterative elaboration leads to distortion of the flow parameters already at first iteration. They are not recovered at the following steps. This fact has been fixed during test calculations of the symmetrical cavitating elliptical foil at zero angle-of-attack. The expected symmetry of the upper and lower cavities is obtained when they are calculated simultaneously and is not in the separate iterative algorithm.

5. Validation and comparisons

At present the developed method is realized in the analysis programs for non-cavitating 3D wings and propellers and in the analysis program for 2D cavitating foils, which allows the prediction of the cavities in the 3D case using the algorithm of the equivalent profile as described in 4.2. The results of the detail calculation/experiment verification of the propeller program for both steady and unsteady cases are presented in Achkinadze et.al. (2001). At the same time the most reliable experimental data on cavity patterns are related to 2D problem. Therefore the different 2D hydrofoils have been studied and calculated results have been compared with experiments as well as with results by other authors in section 5.1. The example on calculation of the cavity ordinates on the 3D wing is given in section 5.2.

5.1. 2D hydrofoils

Fully wetted conditions. Comparison with analytical solution.

In order to illustrate the precision of the developed BEM and convergence of the numerical procedure with increase of the number of the panels the comparison with analytical solution for theoretical Karman-Trefftz profile (camber 1%, thickness 12%, trailing edge angle 15°) has been conducted. The calculated pressure distribution is compared with one obtained from conform mapping solver on the Figure 3. The calculated integral performance (lift and moment coefficients) are compared with analytical solution in Table 1 at different number of the panels. The latter comparison could be considered as test of the integration procedure defining the integral characteristics. In these calculations the position of the MTE panel corresponds to ideal flow theory, i.e. MTE bevel angle is taken according to (25).

a) α=4° **b)** α=–4°

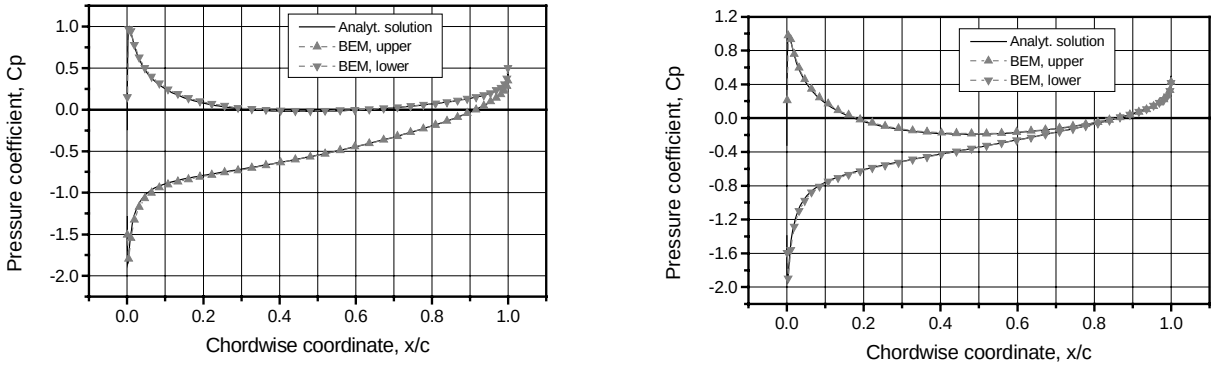

Figure 3. Comparison with analytical solution. Pressure distribution. Karman-Trefftz profile, camber 1%, thickness 12%, trailing edge angle 15°.

Table 1. Comparison with analytical solution. Forces. Karman-Trefftz profile, camber 1%, thickness 12%, trailing edge angle 15°.

a) α=4°

	Analyt.	**M=25**	**M=50**	**M=75**	**M=100**	**M=125**	**M=150**
C_L	0.6158	0.6292	0.6289	0.6286	0.6284	0.6282	0.6282
C_m	0.1132	0.1165	0.1145	0.1138	0.1134	0.1132	0.1132

b) α=–4°

	Analyt.	**M=25**	**M=50**	**M=75**	**M=100**	**M=125**	**M=150**
C_L	-0.3419	-0.3580	-0.3511	-0.3489	-0.3477	-0.3471	-0.3470
C_m	-0.1100	-0.1125	-0.1111	-0.1106	-0.1103	-0.1102	-0.1101

Fully wetted conditions. Comparison with experiment.
The next example shows the "work" of the MTE panel as the tool for approximate accounting for viscous effects. The NACA4412 hydrofoil tested at Re=900000 (Pinkerton (1937)) has been calculated. The first calculation carried out with "ideal" position of the MTE panel, apparently, overpredicts the section lift (see Figure 4 and Table 2). The experimental value of C_L has been used for definition of the corrected β_{MTE} bevel angle according to algorithm (26). As one can see in the both studied cases the resultant pressure distribution appears essentially closer to experimental data. The pitching moment coefficient is also corrected, but full agreement with experiment can not be expected because of tangential stress forces are not captured in the potential solution. Meanwhile the correction of the β_{MTE} bevel angle provides the elaboration of the pressure distribution that is important for prediction of the cavity extent.

a) α=2°, Re=900000 **b)** α=–2°, Re=900000

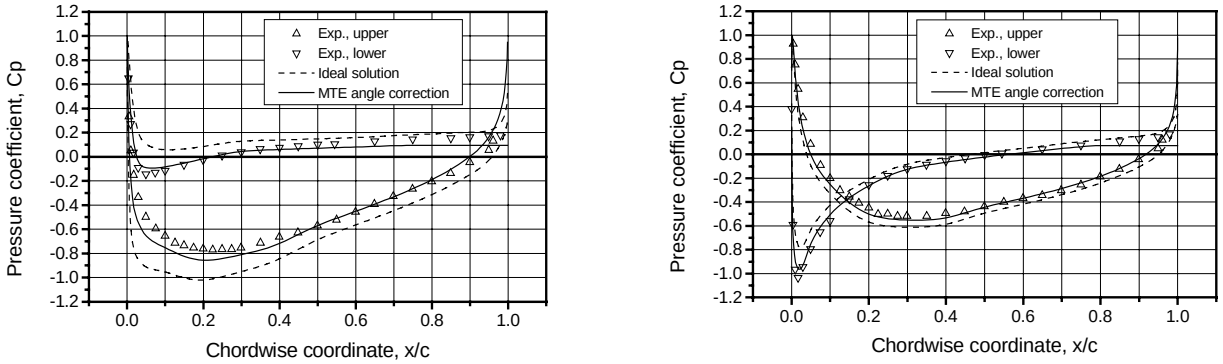

Figure 4. Comparison with experiment. NACA4412. Pressure distribution.

Table 2. Comparison with experiment. NACA4412. Forces. (Closed model)

a) α=2°, Re=900000

	Exp.	Ideal solution	MTE angle correction
C_L	0.520	0.7842	0.520*
$C_{mc/4}$	-0.093	-0.1203	-0.077

* C_L- required value, β_{MTE}=–4.72°

b) α=–2°, Re=900000

	Exp.	Ideal solution	MTE angle correction
C_L	0.162	0.2929	0.162*
$C_{mc/4}$	-0.096	-0.1119	-0.080

* C_L- required value, β_{MTE}=1.94°

NACA16 cavitating foils. Comparison with Riabouchinsky-type model and re-entrant jet model.
The well-known example of NACA16 hydrofoils is considered by many authors as reliable basis and is widely used in testing of the cavity models. In this section the authors compare their results obtained with use of closed model and ICA/FCL procedure with results by Uhlman (1987) (Riabouchinsky-type model with vertical plate) and with results by Dang & Kuiper (1998) who have applied the re-entrant jet model.

Table 3. Comparison of the closed model results with predictions by Uhlman (1987) and Dang & Kuiper (1998) for NACA16 hydrofoils.

a) α=4°, σ=0.87513, (α/σ=0.08)

Profile	Quantity	P2D-CAV	Uhlman	Dang & Kuiper
NACA 16-006	Lcav/c	0.4915	0.490	0.5928
(e_0/c=0.06)	Vcav/c^2	0.0165	0.0170	0.02338
NACA 16-012	Lcav/c	0.5361	0.485	……..
(e_0/c=0.12)	Vcav/c^2	0.0123	0.090	……..
NACA 16-009	Lcav/c	0.5219	0.510	0.5000
(e_0/c=0.09)	Vcav/c^2	0.0147	0.0135	0.0167

Table 3. (continue).

b) $\alpha=4°$, $\sigma=1.0$, $(\alpha/\sigma=0.07)$

Profile	Quantity	P2D-CAV	Uhlman	Dang & Kuiper
NACA 16-006	Lcav/c	0.3521	0.350	0.3917
(e_0/c=0.06)	Vcav/c^2	0.0090	0.0090	0.01106
NACA 16-009	Lcav/c	0.3365	0.330	0.3376
(e_0/c=0.09)	Vcav/c^2	0.0066	0.0060	0.0065
NACA 16-012	Lcav/c	0.3202	0.320	0.2843
(e_0/c=0.12)	Vcav/c^2	0.0046	0.0040	0.00321

c) $\alpha=4°$, $\sigma=1.3$, $(\alpha/\sigma=0.053)$

Profile	Quantity	P2D-CAV	Uhlman	Dang & Kuiper
NACA 16-006	Lcav/c	0.1868	0.185	0.2070
(e_0/c=0.06)	Vcav/c^2	0.0029	0.0030	0.00365
NACA 16-009	Lcav/c	0.1619	0.160	0.1579
(e_0/c=0.09)	Vcav/c^2	0.0016	0.0018	0.00159
NACA 16-012	Lcav/c	0.1271	0.120	……
(e_0/c=0.12)	Vcav/c^2	0.0007	0.000…	……

In the Table 3 the authors' results (P2D-CAV program) from last iteration of the 4th (non-liner) step are given. They have been obtained after elaboration of the cavity detachment point. If summarize the results of the comparisons one can note that good agreement with results by Uhlman is observed for cavity lengths up to 0.5c. For relatively long cavities (Lcav/c>0.6) the discrepancy increases that could be expected, because in this range the closed model does not answer the physics of the flow. It has to be noted that lower boundary of the closed model validation also exists and manifests itself when cavity length is about (0.02-0.03)c. Apparently, such short cavities already can not be simulated by sheet model and they are somewhat like bubbles. From the results presented on the Figure 5 one can infer that widely cited effect of the profile thickness on the cavity length and volume (decrease of the cavity size with increase of the foil thickness, firstly pointed by Uhlman (1987)) is reflected by the model at Lcav/c≤0.40. Then it vanishes or even changes on the opposite (for cavity length). The Uhlman's results confirm this conclusion, in particular.

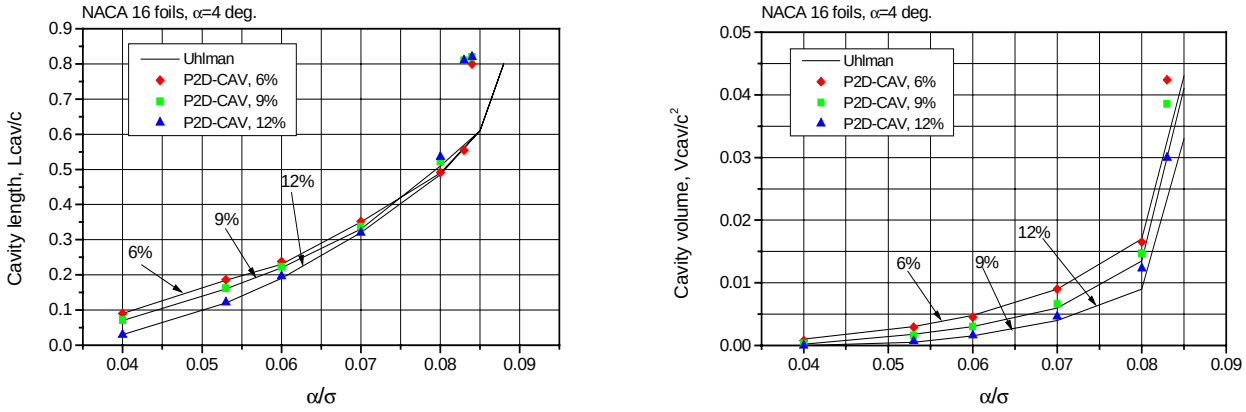

Figure 5. Effect of the foil thickness on cavity length and volume (closed model). Comparison with Uhlman (1987).

The re-entrant jet model by Dang & Kuiper (1998) yields the longer patterns at quite big cavity length and shorter patterns for relatively short cavities in comparison with closed models. In general, it looks like re-entrant jet model makes the above-mentioned foil thickness effect more expressive.

The change of the location of the cavity detachment point after ICA/FCL procedure is shown in the Table 4. Referring on experimental data by Arakeri (1975) one can assume that in the reality the cavity detachment point lies slightly downstream of the location of the fully wetted pressure minimum. It allows the many authors to prescribe the location of the detachment point in the pressure minimum locus or at the leading edge (when angle-of-attack is large). These results are connected with viscous and capillary phenomena (Amromin et.al. (1995)). Nevertheless, it is possible to obtain the qualitative agreement with Arakeri's results even in the ideal solution. Authors' ICA procedure starts with cavity detachment point defined from $-Cp=\sigma$ condition and then elaborates it in iterations using Brillouin-Villat condition. As one can see from Table 4 the calculated detachment point indeed appears after fully wetted pressure minimum locus. The greatest displacement of the detachment point from initial position has been fixed for 12%-thickness (the most thick) foil. This fact is also in agreement with conclusions by Uhlman (1987). Authors' calculations show that displacement of the cavity detachment point is greater at small angles-of-attack for given foil.

Table 4. Displacement of the cavity detachment point after iterative elaboration of the detachment condition.

	Chordwise coordinate, ξ/c
NACA 16-006	
Check at fully wetted conditions	0.4999
Fully wetted pressure minimum	0.4999
Final location after ICA procedure	0.4994
Displacement from initial locus	0.0005c
NACA 16-009	
Check at fully wetted conditions	0.4999
Fully wetted pressure minimum	0.4994
Final location after ICA procedure	0.4984
Displacement from initial locus	0.0015c
NACA 16-012	
Check at fully wetted conditions	0.4999
Fully wetted pressure minimum	0.4969
Final location after ICA procedure	0.4969
Displacement from initial locus	0.0030c

NACA16 cavitating foils. Comparison with experiments by Franc & Michel.

The cavity patterns on the 12%-thickness NACA16 hydrofoils tested by Franc & Michel (1985) have been studied numerically in Rowe & Blottiaux (1993) using different cavity closure models. Their conclusions were about unsatisfactory prediction by closed model. The improved open cavity models were referred as more preferable for this particular case. The authors' calculations have revealed the crash of the closed scheme when cavitation number becomes less than σ=1.1-1.2 for α=5° and σ=1.2 for α=6°. Above these values the closed model allows the converged results, which are compared with Rowe & Blottiaux predictions in the Table 5. The open model has been used for calculations in the considered case and results of the theory/experiment comparisons are presented in the Table 6 and on the Figure 6.

Table 5. Comparison of the cavity lengths (closed model) with predictions by Rowe & Blottiaux for NACA16 hydrofoils.

a). α=5°

Cavitation number	**P2D-CAV**	**Rowe & Blottiaux**
σ=1.2	0.240	0.270
σ=1.4	0.382	0.450

b). α=6°

Cavitation number	**P2D-CAV**	**Rowe & Blottiaux**
σ=1.3	0.523	……
σ=1.4	0.413	0.460
σ=1.5	0.337	0.360

Table 6. Comparison of the cavity lengths (open model) with experiments by Franc & Michel (1985) for NACA16 hydrofoils. α=5°.

Cav. Number	**Linearized step**	**Non-linear step, end panel**	**Non-linear, zone of the recovered pressure**	**Exp.**
σ=1.4	0.088	0.081	0.110	…..
σ=1.2	0.142	0.118	0.150	…..
σ=1.0	0.240	0.203	0.260	0.18
σ=0.9	0.315	0.275	0.330	0.30
σ=0.8	0.395	0.353	0.430	0.47
σ=0.7	0.582	0.520	0.640	0.66
σ=0.6	0.756	0.756	0.805	0.85
σ=0.5	0.870	0.820	0.880	0.97

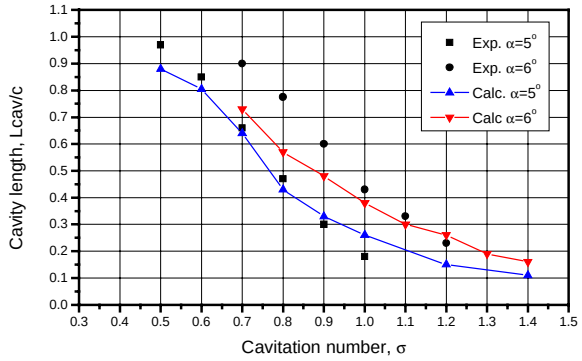

Figure 6. Comparison of the cavity lengths predicted by the open model with experiments by Franc & Michel (1985) for NACA16 hydrofoils.

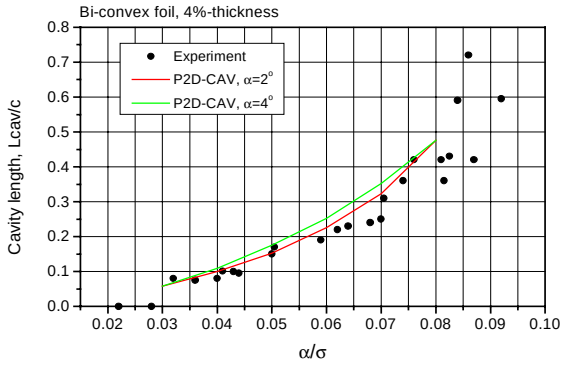

Figure 7. Comparison of the cavity lengths predicted by the closed model with experiments by Meijer (1959) for 4%-thickness biconvex hydrofoil.

In general, the prediction was better for α=5° case. Analysis of the pressure distributions obtained on the linearized and non-linear steps reveals the jump of the pressure after cavity end panel at the non-liner step. Presumably, it is caused by hollow space between cavity bound and foil surface, where are no singularities and boundary conditions, and is the consequence of the discretization. This effect does not appear at the linearized step and becomes less with more fine grid. The reasonable question arises: how to define the cavity length in this case? The oscillating pressure domain could be thought as domain of the collapsing cavity tail. If include the zone where oscillating pressure recovers to the vapour pressure in the cavity, the cavity always appears longer and closer to linearized step prediction as one can see from Table 6.
The comparison of the cavity lengths and volumes and lift coefficients predicted by open and closed models is presented in the Table 7 for σ=1.2 when closed model allows the converged solution. Obviously, the difference between linearized and fully non-liner steps is essentially less for open model in terms of all compared parameters.

Table7. Comparison between open and closed model results for NACA16 hydrofoils. σ=1.2, α=5°.

Model	**Lcav/c Linea-rized**	**Vcav/c^2 Linea-Rized**	**C_L Linea-rized**	**Lcav/c Non-linear**	**Vcav/c^2 Non-linear**	**C_L Non-linear**
Closed	0.539	0.0162	0.809	0.382	0.0087	0.660
Open	0.142	0.0017	0.633	0.118	0.0010	0.630

Biconvex cavitating foils. Comparison with experiments by Meijer.
The Meijer's (1959) experimental data on 4%-thickness biconvex hydrofoil are also commonly used in 2D cavity pattern comparisons. Although many authors beginning from Uhlman (1987) say about too large scatter of the experimental points in this example, it could be useful for estimation of the robustness of the method. The cavity patterns predicted by open model appear very short in comparison with experiment while closed scheme gives the reasonable prognosis. These conclusions are illustrated by the data on the Figure 7. The results of the closed model calculation could be estimated as satisfactory up to Lcav/c=0.45 at least.

5.2. 3D wings

NACA0015-type cavitating wing. Comparison with experiments by SRI.
The developed 2D cavitation program in couple with 3D non-cavitating wing code and method of the equivalent 2D profile described in 4.2 has been applied to prediction of the cavity ordinates at the midspan section of the 3D rectangular wing (aspect ratio 4.0) having NACA0015 sections. The experimental data on this wing tested in SRI has been borrowed from Kai & Ikehata (1998). The calculated cavity patterns are presented on Figure 8 along with experimental points for three different cavitation numbers at equal angle-of-attack α=8°. They have been obtained using closed cavity model at 4th –step final non-linear iteration. The equivalent angle-of-attack amount 5.8° in this case.

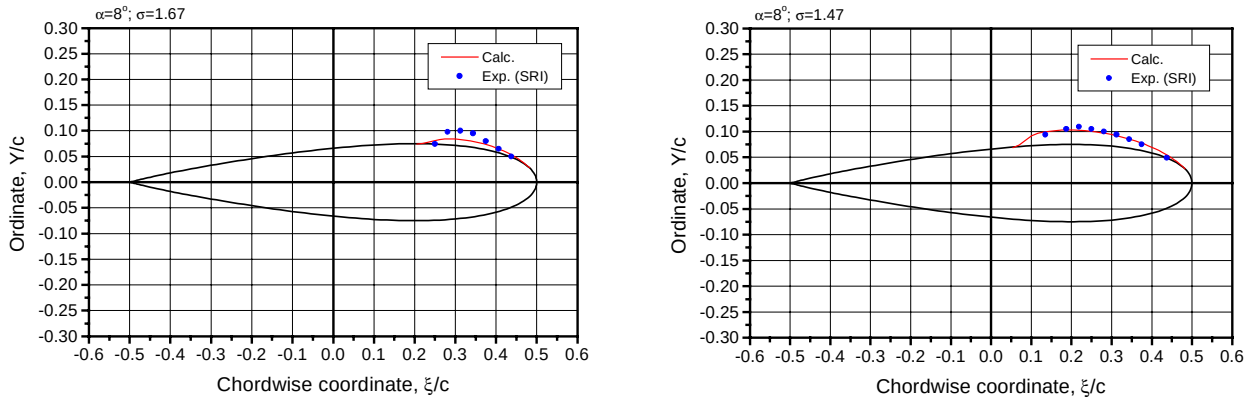

Figure 8. Comparison of the calculated cavity ordinates with experiment by SRI on NACA0015 3D wing.

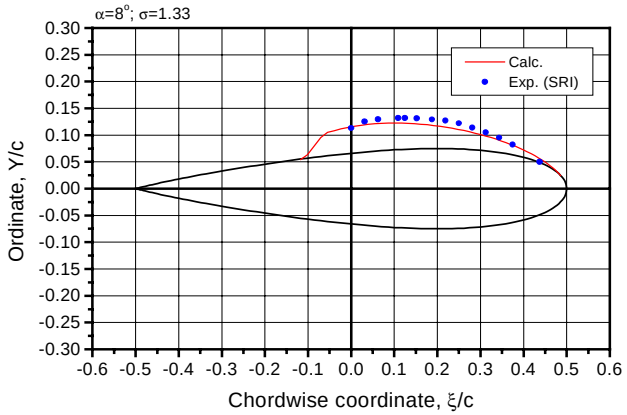

Figure 8. (continue)

The satisfactory prediction of the cavity ordinates and lengths could be seen. The significant effect of the location of the cavity detachment point has taken place in this example. Presumably, the proper elaboration of the cavity detachment point from Brillouin-Villat condition during ICA-procedure has allowed to capture the effect of the thick leading edge and to achieve the better agreement with experiment in comparison with Kai & Ikehata (1998) who start the cavity from leading edge.

6. Conclusions

A new velocity based BEM with Modified Trailing Edge (MTE) has been developed and applied to prediction of the partial cavities on the wings and propeller blades. The mathematically correct formulation allows us to consider this method as very useful for numerical simulation of the cavitating bodies.

Algorithm of the MTE directly satisfies the Kutta-Jowkovski's condition unlike unavoidable iterative procedure in the potential based BEM. MTE is the tool for approximate accounting for viscous effects on pressure distribution.

The using of the curvilinear boundary elements and accurate approximation of the section edges are the essential advances of a method in the 3D case.

In authors opinion the Iterative Cavity Alignment (ICA) procedure with Free Cavity Length (FCL) and miscellaneous (closed/open) cavity closure model are the most efficient in the practical calculations.

The performed verification has shown the robustness of a method and the obtained results are in satisfactory agreement with experiments and with results of the other authors.

The extension of the numerical procedure on full 3D solution of the cavitating flow around propeller blade (including super-cavitation) is seen as the main future task.

Acknowledgements

This work is a part of the post-doctoral research study of the second author in MARINTEK Sintef Group, Trondheim, Norway. It is sponsored by SKIPRO2001 Research Program organized by Research Council of Norway.

References

ACHKINADZE, A.S. 2001 Supercavitating propellers. In *Preprints: Lecture Series Monographs, Von Karman Institute for Fluid Dynamics, RTO AVT/VKI Special Course: "Supercavitating Flows"*, Rhode-Saint-Genese, Belgium, February 12-16.

ACHKINADZE, A.S., BERG, A., KRASILNIKOV, V.I. & STEPANOV, I.E. 2001 Numerical and Experimental Verification of the SPA/QSPA-POD Velocity Based BEM Program for Steady and Quasi-Steady Analysis of the Podded Propellers. Paper submitted on *SP'2001 Conference (Lavrentiev's Lectures), St Peterburg, Russia*, June 19-21.

ACHKINADZE, A.S. & FRIDMAN, G.M. 1994 Artificial Variation Problems Method for Three-Dimensional Lifting Cavity Forms. In *Trans. of 12th Symposium on Naval Hydrodynamics*, 212-222, University of California, Santa Barbara, USA, August 21-26.

ACHKINADZE, A.S. & FRIDMAN, G.M. 1998 A New Algorithm for Numerical Investigation of Unsteady Cavitating Screw Propeller with Use of Variation Approach. In *Proc. 3rd International Symposium on Cavitation*, vol.1, 279-284, Grenoble, France, April 7-10.

ACHKINADZE, A.S. & KRASILNIKOV, V.I. 2001 A New Velocity Based BEM for Analysis of the Non-cavitating and Cavitating Propellers and Foils. Paper submitted on *SP'2001 Conference (Lavrentiev's Lectures)*, St Peterburg, Russia, June 19-21.

ACHKINADZE, A.S. & NARVSKY, A.S. 1980 Linear Open Cavity Model for Calculation of the Cavitating Wings at Arbitrary Cavitation Number. In *Proc. "Dynamics of the continuous fluid with free surface"*, 10-15, Cheboksary, (in Russian).

ACHKINADZE, A.S. & NARVSKY, A.S. 1987 Calculation of Cavitating Propellers Based on the Lifting-Surface Theory. In *Proc. 4th International Congress IMAEM*, vol.5, 158/1-15, BSHC, Varna, Bulgaria, May 25-30.

ALEXANDROV, K.V. 1978 Partially Cavitating Foil of Arbitrary Geometry. In *Trans. of NTO Sudprom*, vol.284, 73-80. (in Russian).

AMROMIN, E.L., VASILIEV, A.V. & SYRKIN, E.N. 1995 Propeller Blade Cavitation Inception Prediction And Problems of Blade Geometry Optimization: Recent Research at the Krylov Shipbuilding Research Institute. *Journ. of Ship Research*, vol.39, No.3, 202-212.

ANDO, J., MAITA, S. & NAKATAKE, K. 1998 A New Surface Panel Method to Predict Steady and Unsteady Characteristics of Marine Propeller. In *Preprints of 22nd Symposium on Naval Hydrodynamics*, Washington, D.C., August 9-14, Preprints, Monday Session.

ARAKERI, V.H. 1975 Viscous Effects on the Position of Cavitation from Smooth Bodies. *Journ. of Fluid Mechanics*, vol.68, 779-799.

DANG, J. & KUIPER, G. 1998 Re-Entrant Jet Modeling of Partial Cavity Flow on Two-Dimentional Hydrofoils. In *Proc. 3rd International Symposium on Cavitation*, vol.2, 233-242, Grenoble, France, April 7-10.

FRANC, J.P. & MICHEL, J.M. 1985 Attached Cavitation and the Boundary Layer: Experimental Investigation and Numerical Treatment. *Journ. of Fluid Mechanics*, vol.154, 63-90.

GEURST, J.A. 1956 Linearized Theory for Partially Cavitated Hydrofoils. *International Shipbuilding Progress*, vol.6, No.60, 369-384.

HESS, J.L. & VALAREZO, W.O. 1985 Calculation of Steady Flow About Propellers by Means of a Surface Panel Method. In *29th Aerospace Sciences Meeting, AIAA, Reno*, Nevada, January.

HSIAO, C.T. & Pauley, L.L. 1998 Numerical Computation of Tip Vortex Flow Generated by a Marine Propeller. *ASME Fluids Engineering Division Summer Meeting, FEDSM'98*, Washington, D.C.

ISHII, N. 1992 Prediction of Propeller Performance and Cavitation Based on the Numerical Modeling of Propeller Vortex System. In *Proc. International Symposium on Propeller and Cavitation*, Hamburg, Germany, 33-41.

ITTC Committee. 1999 Final Report and Recommendations to the 22nd ITTC. The Specialists Committee on Computational Method for Propeller Cavitation. In *Proc. of 22nd ITTC*, vol.II, 433-463, September 5-11.

IVANOV, A.N. 1980 *Hydrodynamics of the Cavitating Flows*. Sudostroenie, Leningrad. (in Russian).

KAI, H. & IKEHATA, M. 1998 Numerical Simulation of Cavitation on 3-Dimensional Wings and Marine Propeller by a Surface Vortex Lattice Method. In *Proc. 3rd International Symposium on Cavitation*, vol.2, 281-286, Grenoble, France, April 7-10.

KIM, Y.-G. 1995 Prediction of Unsteady Performance of Marine Propellers with Cavitation Using a Surface Panel Method. Ph.D. Thesis, Dept. of Naval Architecture and Ocean Engineering, Chungnam National University, Korea.

KINNAS, S.A. 1998 The Prediction of Unsteady Sheet Cavitation. In *Proc. 3rd International Symposium on Cavitation*, vol.1, 19-36, Grenoble, France, April.

KINNAS, A.S. & FINE, N.E. 1993 Numerical Nonlinear Analysis of the Flow Around Two- and Three- Dimensional Partially Cavitating Hydrofoils. *Journ. of Fluid Mechanics*, vol.254.

KOCHIN, N.E., KIBEL, I.A. & ROZE, N.V. 1963 *Theoretical Hydromechanics*. Part I, 583, 1963.

LEE, C.-S. 1979 Prediction of Steady and Unsteady Performance of Marine Propellers With and Without Cavitation by Numerical Lifting Surface Theory. Ph.D. Thesis, Dept. of Ocean Engineering, MIT.

LEE, J.-T. 1987 A Potential Based Panel Method for the Analysis of Marine Propellers in Steady Flow. Report 87-13, Dept. of Ocean Engineering, MIT, July.

LEMONNIER, H. & ROWE, A. 1988 Another Approach in Modeling Cavitating Flows. *Journ. of Fluid Mechanics*, vol.195, 557-580.

MASLOV, L.A. 1974 Potential Flow Around Finite-Span Wing with Arbitrary Section Profile. In *Trans. of TSAGI*, vol.1567. (in Russian)

MEIJER, M.C. 1959 Some Experiments on Partly Cavitating Hydrofoils. *International Shipbuilding Progress*, vol.6, No.60, August.

MISHKEVICH, V.G. 1994 Design of Marine Propellers Using Vortex Theory: Theory and Practice. In *Proc. Propellers/Shafting'94 SNAME Symposium, Virginia Beach, VA*, September 20-21.

MISHKEVICH, V.G. 1997 Flow Around Marine Propeller: Nonlinear Theory Based on Vector Potential. In *Proc. Propellers/Shafting'97 SNAME Symposium, Virginia Beach, VA*, September 23-24.

MUELLER, A.C. & KINNAS, A.S. 1997 Cavitation Prediction Using a Panel Method. In *Proc. ASME Symposium on Marine Hydrodynamics and Ocean Engineering*, Dallas, USA.

NARAYANA, C.L. 1998 Panel Method Calculation for the DTMB4119 Propeller for the 22nd ITTC Propulsion Committee Propeller RANS/Panel Method Workshop. In *22nd ITTC Propulsion Committee Propeller RANS/Panel Method Workshop*, 351-370, Grenoble, France, April 5-6.

PINKERTON, R.M. 1937 The Variation with Reynolds Number of Pressure Distribution over an Airfoil Section. Report No.613, N.A.C.A., Langley Field, VA, July.

REBOUND, J.L. & DELANNOY, Y. 1994 Two-Phase Flow Modeling of Unsteady Cavitation. In *Proc. 2nd International Symposium on Cavitation*, Tokyo, Japan.

ROWE, A. & BLOTTIAUX, O. 1993 Aspects of Modeling Partially Cavitating Hydrofoils. *Journ. of Ship Research*, vol.37, No.1, 34-48.

SZANTYR, J.A. 1994 A Method for Analysis of Cavitating Marine Propellers in Nonuniform Flow. *International Shipbuilding Progress*, vol.41, No.427, 267-288.

UHLMAN, J.S. 1987 The Surface Singularity Method Applied to Partially Cavitating Hydrofoils. *Journ. of Ship Research*, vol.31, No.2.

YAMAGUCHI, H. & KATO, H. 1983 On Application of Nonlinear Cavity Flow Theory to Thick Foil Sections. In *Proc. Second International Conference on Cavitation, IMechE*, 167-174.

ZAVADOVSKY, N.Y. & RUSETSKY, A.A. 1988 Application of the Linear Lifting-Surface Theory to Analysis of the Cavitating Propellers with Complex Blade Geometry. In *Sudostroitelnaya promyshlennost, Ser.: Proektirovanie Sudov*, vol.7, 47-51, (in Russian).